Materials Science and Engineering A 532 (2012) 500–504

Contents lists available at SciVerse ScienceDirect

Materials Science and Engineering A

journal homepage: www.elsevier.com/locate/msea

Orientation-dependent indentation modulus and yielding in a high Mn twinning-induced plasticity steel

Singon Kang[a], Yeon-Seung Jung[a], Byung-Gil Yoo[b], Jae-il Jang[b], Young-Kook Lee[a,*]

[a] Department of Materials Science and Engineering, Yonsei University, Seoul 120-749, Republic of Korea
[b] Division of Materials Science and Engineering, Hanyang University, Seoul 133-791, Republic of Korea

ARTICLE INFO

Article history:
Received 23 June 2011
Received in revised form 5 October 2011
Accepted 24 October 2011
Available online 11 November 2011

Keywords:
Nanoindentation
High Mn steel
Elastic modulus
Mechanical twinning
Surface orientation

ABSTRACT

The dependencies of indentation modulus and yielding behavior on the crystallographic orientation in a high Mn twinning induced plasticity (TWIP) steel were systematically investigated by spherical nanoindentation. A series of nanoindentation experiments revealed that the values of the plane-strain modulus and maximum shear stress at the pop-in increased with an order of (0 0 1), (1 0 1), and (1 1 1) grains. Mechanical twins were only observed in the indented (0 0 1) grains, as was expected from Schmid factor for twinning in fcc crystals.

1. Introduction

The crystallographic orientation is known to be one of the most important factors for the mechanical properties and deformation behaviors of crystalline metals and alloys. In a single crystalline high Mn Hadfield steel with a chemical composition of Fe–12.34 wt.%Mn–1.03 wt.%C, tension and compression experiments showed that true stress–strain curve and deformation mechanism significantly depends on the crystallographic orientation parallel to the deformation axis [1]. When the tensile axis was [1 1 1] and the compressive axis was [0 0 1], the mechanical twinning played an important role as a predominant deformation mechanism at the onset and early stage of plastic flow, whereas the dislocation slip governed the plastic deformation when the tensile axis was [0 0 1] or [1 2 3] and the compressive axis was [1 1 1] or [1 2 3].

In high Mn twinning-induced plasticity (TWIP) steel [2], the orientation-dependent deformation behavior has also been investigated mainly through tension and compression tests [3,4]. Yang et al. [3] suggested that mechanical twinning occurred primarily at the [1 1 1]-oriented grains parallel to the tensile axis in a polycrystalline Fe–33Mn–3Al–3Si TWIP steel, while Meng et al. [4] reported that the [0 0 1]-oriented grains parallel to the compressive axis exhibited active mechanical twinning. However, despite the increased interest in high Mn austenitic steel, little information is available about the orientation-dependencies of its elasticity and plastic deformation behavior.

Meanwhile, the crystallographic anisotropy of mechanical properties in some metallic materials has often been explored through nanoindentation experiments. For example, the reduced modulus of (0 0 1) surface in some fcc metals such as Cu, Al, and 316L stainless steel exhibited a large difference from that of (1 1 1) surface by about 10% [5,6]. The orientation-dependence of the surface morphology after indentation was systematically reported in a single crystal sample of fcc Cu by Wang et al. [7] and tetragonal γ-TiAl by Zambaldi et al. [8] in relation to the primary slip system. In addition, for better understanding of indented microstructure, 3-dimensional observations below the indent were done in a single crystal sample of fcc Cu [9,10].

In the present study, a series of nanoindentation and electron back-scattered diffraction (EBSD) tests were performed to investigate the orientation-dependent deformation characteristics such as elasticity, shear yield stress, and the morphology of the indented surface in a polycrystalline high Mn TWIP steel. The deformation mode is discussed in terms of competition between dislocation glide and mechanical twinning.

2. Experimental procedure

The high Mn TWIP steel sheets of 1.2 mm thick, whose chemical composition of Fe–17.5Mn–0.58C–1.5Al in weight percent were prepared by vacuum induction melting, homogenization, hot

* Corresponding author. Tel.: +82 2 2123 2831; fax: +82 2 312 5375.
E-mail address: yklee@yonsei.ac.kr (Y.-K. Lee).

0921-5093/$ – see front matter © 2011 Elsevier B.V. All rights reserved.
doi:10.1016/j.msea.2011.10.116

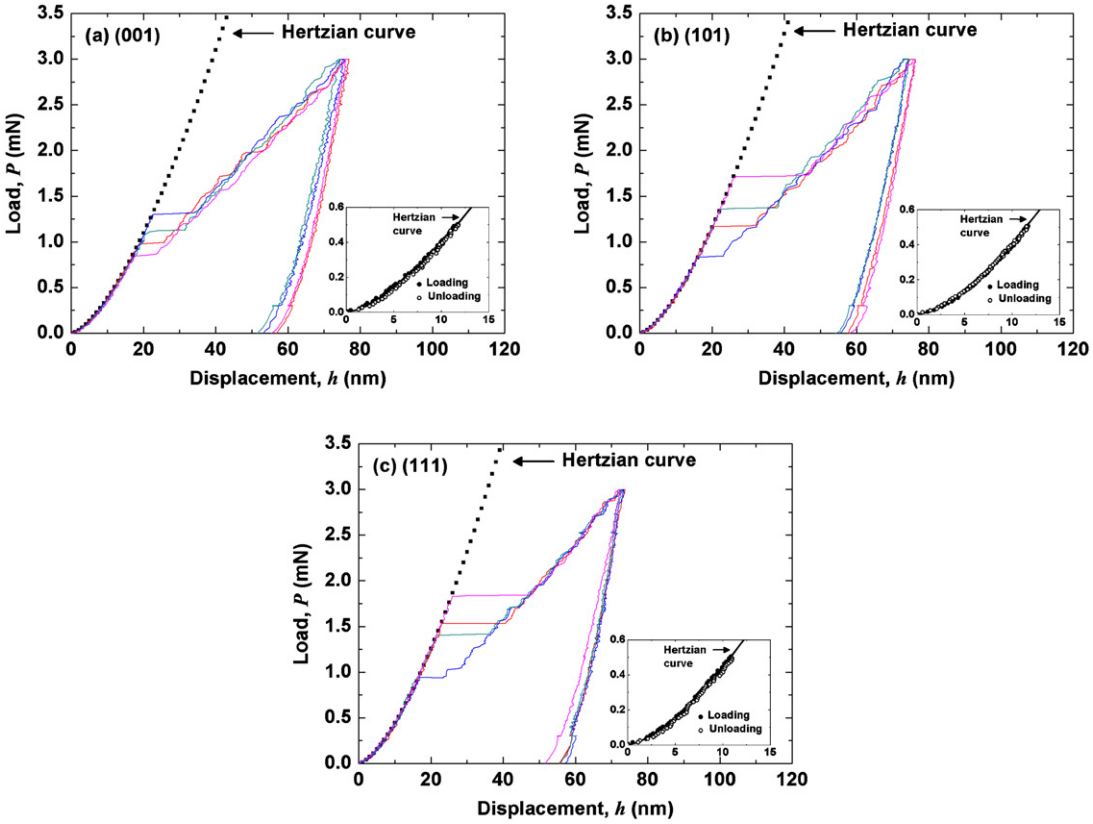

Fig. 1. Load–displacement curves of (a) (0 0 1), (b) (1 0 1), and (c) (1 1 1) grains in Fe–18Mn–0.6C–1.5Al TWIP steel using a spherical indenter of 3.3 μm in radius. The load–displacement curves in small boxes are the elastic deformation region.

rolling, and cold rolling [11]. To obtain fully recrystallized austenite single phase samples, the cold-rolled sheets were annealed at 1100 °C for 10 min using a vacuum tube furnace.

The annealed specimens were mechanically polished using emery papers, diamond suspension, and finished with colloidal silica particles. The surface orientations of the grains in the specimen were observed using an EBSD equipment (Oxford instrument, INCA Crystal) attached to a field-emission scanning electron microscope (FE-SEM, JEOL, JSM7001F).

Nanoindentation tests were performed on the EBSD-examined surface using a Nanoindenter-XP (MTS System Corp.) under a peak load (P_{max}) of 3 mN using a conical indenter with a spherical tip of 3.3 μm in radius instead of a tip-blunted Berkovich indenter. An array of indents of 15 × 15 matrix was defined with an indent gap of 20 μm. Subsequently FE-SEM images of the indented surface were taken. To avoid the grain boundary strengthening effect, the indents made near grain boundaries were excluded.

The cross-sectional analysis of the indented surface was performed using a transmission electron microscope (TEM, FEI, Tecnai F20) operated at 200 kV. The TEM samples perpendicular to the indented surface were prepared by a focused ion beam (FIB, FEI, Helios) milling.

3. Results and discussion

Fig. 1 shows the representative load (P)–displacement (h) curves recorded during spherical nanoindentation tests of each grain with a surface orientation of (0 0 1), (1 0 1), and (1 1 1), respectively in the polycrystalline fcc TWIP steel specimen. Each P–h curve shows a large displacement excursion (so called 'pop-in') during loading sequence and the displacement was not fully recovered upon unloading. The loading part before the pop-in matches well with a fully elastic curve obtained with a lower peak load like P_{max} = 0.5 mN (see the inset figure where the P–h curves for both loading and unloading are completely overlapped). This implies that the deformation prior to the pop-in is fully elastic. The elastic part of each P–h curve is well described by a Hertzian elastic contact solution [12]

$$P = \frac{4}{3} E_r \sqrt{Rh^3} \tag{1}$$

where R is the radius of a spherical indenter (3.3 μm) and E_r is the reduced modulus affected by the elastic moduli of both indenter and specimen. From Eq. (1) and the measured P–h curve of the elastic part, E_r can be calculated for each orientation; 156.2, 162.6, and 170.8 GPa in (0 0 1), (1 0 1), and (1 1 1) orientations, respectively. Subsequently, the plane-strain modulus, $E_s/(1-\nu_s^2)$, for each orientation is calculated using the E_r as follows:

$$\frac{E_s}{1-\nu_s^2} = \left(\frac{1}{E_r} - \frac{1-\nu_i^2}{E_i} \right)^{-1} \tag{2}$$

where E is the elastic modulus, ν is Poisson's ratio, and subscripts i and s indicate the indenter and specimen, respectively. With E_i = 1141 GPa and ν_i = 0.07 for a diamond indenter [13], the average values of $E_s/(1-\nu_s^2)$ for (0 0 1), (1 0 1), and (1 1 1) grains were calculated to be 180.8, 189.5, and 200.7 GPa, respectively, as given in Fig. 2a. These values are reasonably close to the plane-strain modulus (~185 GPa) of a polycrystalline bulk TWIP steel sample, which was determined with the known bulk elastic properties of this TWIP steel; E_s = 173.8 GPa and ν_s = 0.24 [14].

The increase in E_s with an order of (0 0 1), (1 0 1), and (1 1 1) can be rationalized by taking into consideration the compliances of a cubic crystal system [6]. For a grain having [h k l]-direction parallel

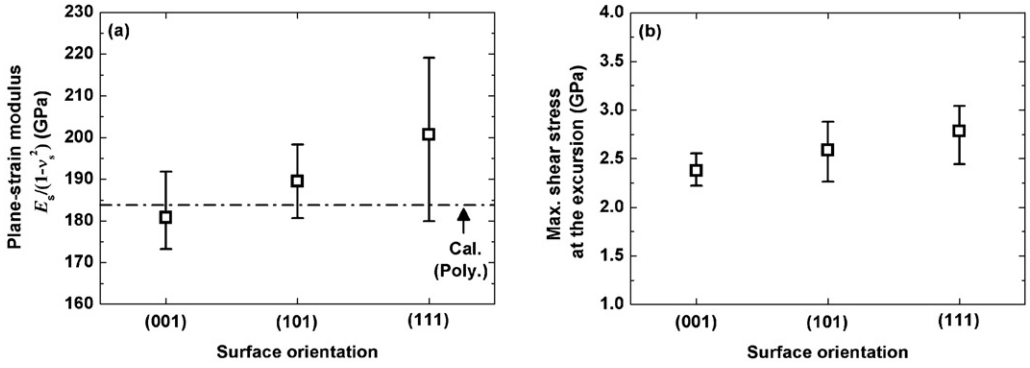

Fig. 2. (a) The plane-strain modulus of three different orientations. Dashed line represents the calculated value using the elastic properties of bulk polycrystalline Fe–18Mn–0.6C–1.5Al TWIP steel. (b) The maximum shear stresses at the excursion in the three different orientations.

to the loading axis, the dependence of the elastic modulus (E_{hkl}) upon an anisotropy factor A_{hkl} is

$$\frac{1}{E_{h\,k\,l}} = S_{11} + (2S_{12} - 2S_{11} + S_{44})A_{hkl} \tag{3}$$

where S_{11}, S_{12}, and S_{44} are three independent compliances of a cubic system, and A_{hkl} is given as

$$A_{h\,k\,l} = \frac{h^2k^2 + k^2l^2 + l^2k^2}{(h^2 + k^2 + l^2)^2} \tag{4}$$

and thus, $A_{0\,0\,1}$, $A_{1\,0\,1}$, and $A_{1\,1\,1}$, are 0, 1/4, and 1/3, respectively. Very recently, Stinville et al. [6] calculated the elastic modulus of fcc 316L stainless steel using S_{11}, S_{12}, and S_{44} of 10.7×10^{-3}, -4.25×10^{-3}, and 8.6×10^{-3} GPa^{-1}, and showed that the $E_{1\,1\,1}$ is much higher than $E_{0\,0\,1}$, which is in an agreement with our result.

Now, turning our attention to the yielding, the maximum shear stress at the onset of the excursion (pop-in), τ_{max} is calculated by [12]

$$\tau_{max} = 0.31\left(\frac{6E_r^2}{\pi^3R^2}P\right)^{1/3} \tag{5}$$

The calculated τ_{max} values of different surface orientations, plotted in Fig. 2b, shows that τ_{max} is 2.38 ± 0.16, 2.59 ± 0.31, and 2.79 ± 0.30 GPa for (0 0 1), (1 0 1), and (1 1 1) respectively. The value is clearly increasing with an order of (0 0 1), (1 0 1), and (1 1 1). The values are much higher than the expected values ($\tau_y \sim \sigma_y/2$) from macroscopic tension or compression tests, possibly due to a whisker-like effect: the stressed zone contains few pre-existing dislocations [15]. Meanwhile, the orientation dependency of τ_{max} agrees well with that of compressive yield strength in a high Mn Hadfield steel whose yield strength is 313 MPa for [0 0 1] loading axis and 425 MPa for [1 1 1] loading axis [1].

The orientation-dependency of uniaxial yield strength has often been analyzed in terms of the Schmid factor. The higher the Schmid

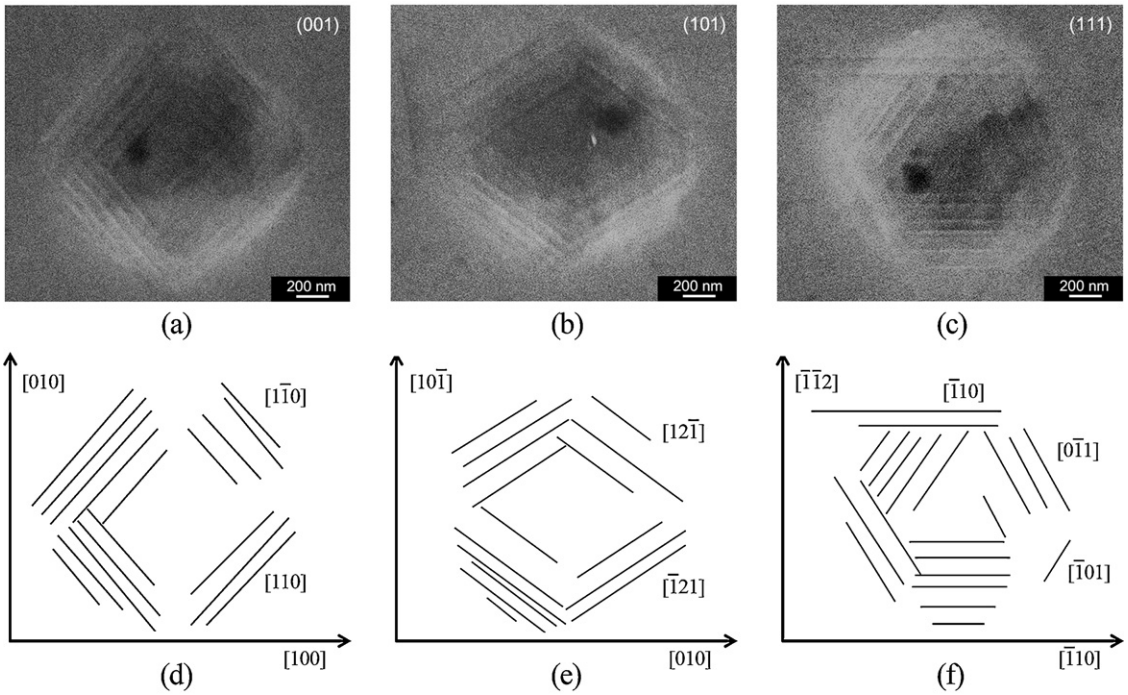

Fig. 3. Scanning electron microscopic (SEM) images of the indented surfaces of (a) (0 0 1), (b) (1 0 1), and (c) (1 1 1) grains and their schematics of (d) (0 0 1), (e) (1 0 1), and (f) (1 1 1), respectively.

Table 1
Maximum Schmid factors for three different orientations of [0 0 1], [1 0 1], and [1 1 1] under compression for dislocation slip and mechanical twinning.

Deformation mode	Orientation		
	[0 0 1]	[1 0 1]	[1 1 1]
Dislocation slip	0.41	0.41	0.28
Mechanical twinning	0.47	0.25	0.16

factor, the lower the yield strength. Although the stress state under the indenter is much more complicated than the uniaxial condition, one may gain a clue for understanding the anisotropic yielding behavior assuming that the yielding mechanism for the indentation is similar to that for uniaxial compression if the loading axis of indentation is in the same direction as that of compression. Note that in the nanoindentation experiments using a spherical indenter, it was reported that the loading axis of the highly stressed zone was equal to that of the compression tests [16]. Also in a previous nanoindentation study, the compressive Schmid factor was used in each slip system to understand dislocation slip behavior in a single crystal fcc Cu sample indented by a conical indenter [9]. Table 1 lists the maximum Schmid factors for both dislocation slip and mechanical twinning using a preferred slip system of $\{1\,1\,1\}/\langle 1\,1\,0\rangle$ and $\{1\,1\,1\}/\langle 1\,1\,2\rangle$, respectively, when compressive stress is applied in a direction perpendicular to each surface of three differently oriented grains of fcc metals.

From Table 1, it is expected that during the nanoindentation test, the dislocation slip or mechanical twinning can occur more easily in (0 0 1) grains rather than in (1 0 1) and (1 1 1) grains. However, although the maximum Schmid factor for dislocation slip for [0 0 1] is equal to that for [1 0 1], the τ_{max} of (0 0 1) is smaller than that of (1 0 1). In addition, because the maximum Schmid factor for mechanical twinning of [0 0 1] is larger than that of [1 0 1], it is required to investigate the role of mechanical twinning on τ_{max}.

If one adopts an assumption that the critical resolved shear stresses for both slip and twinning are approximately the same, as in a previous study on the effect of grain orientation on deformation twinning in a high Mn TWIP steel [17], mechanical twinning is expected to occur before dislocation slip in the (0 0 1) grains during the nanoindentation test. In order to investigate the deformation mechanism (slip or twinning) in each orientation, we attempted to examine whether or not the mechanical twinning occurs during the indentation for each surface orientation.

Fig. 3 shows typical SEM images of indented surfaces of (0 0 1), (1 0 1), and (1 1 1) grains and their schematics. The indented surface revealed deformation patterns with fourfold, twofold, and sixfold symmetries for (0 0 1), (1 0 1), and (1 1 1) grains, respectively. This result is similar to that in a Cu single crystal observed by Wang et al. [7]. However, since they used a self-similar sharp indenter that produced a much deeper displacement, it was difficult to observe the detailed morphology of the contact region of the indent. For the indented surface of (0 0 1) grain, as shown in Fig. 3a and d, the primary slip plane $\{1\,1\,1\}$ intersects the indented surface along the [1 1 0] and $[1\,\bar{1}\,0]$ directions, implying that the trace of either dislocation slip or mechanical twinning is given as the fourfold in-plane symmetry along the [1 1 0] and $[1\,\bar{1}\,0]$ on the indented surface of (0 0 1) grain. For the indented (1 0 1) grain (see Fig. 3b and e), the primary slip plane $\{1\,1\,1\}$ crosses the indented surface along the $[\bar{1}\,2\,1]$ and $[1\,2\,\bar{1}]$ orientations, which caused the twofold in-plane symmetry. Lastly, for the indented surface of (1 1 1) grain, the primary slip plane $\{1\,1\,1\}$ intersects the indented surface along the $[\bar{1}\,1\,0]$, $[0\,\bar{1}\,1]$, and $[\bar{1}\,0\,1]$ crystallographic lines, as shown in Fig. 3c and f. Therefore, it is clear that the deformation patterns on the indented surfaces greatly depend on crystallographic orientation.

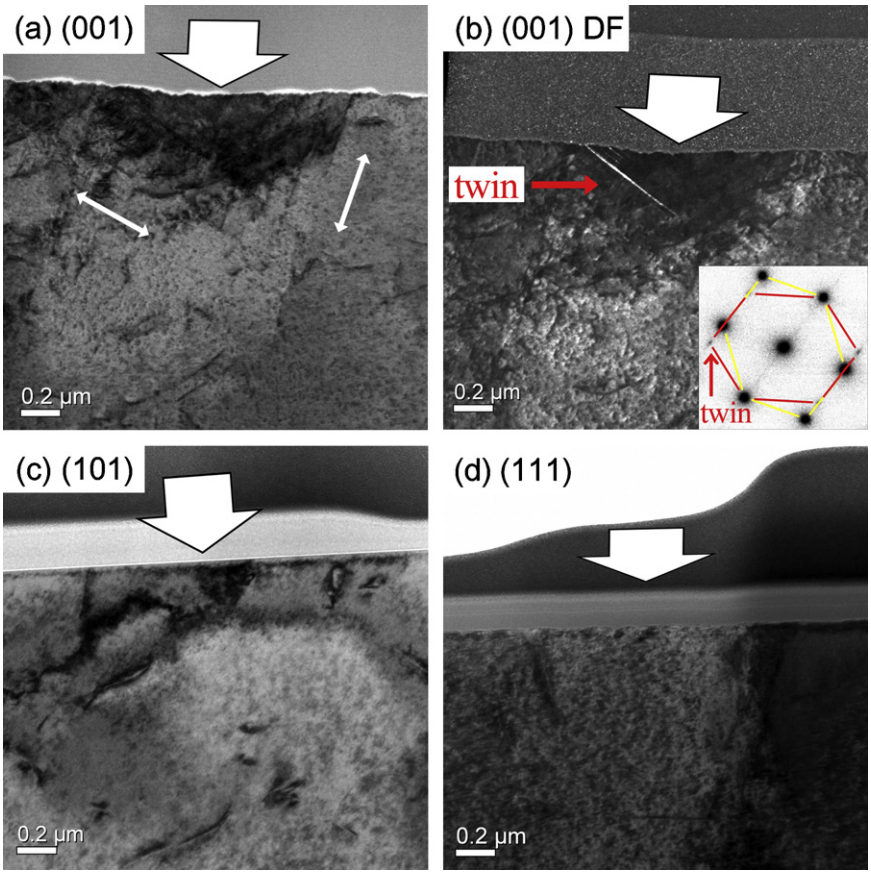

Fig. 4. (a) Transmission electron microscopic (TEM) image of the cross-sectional areas of the grains of (0 0 1) oriented surfaces, and (b) its dark field image alongside a diffraction pattern of twins. Those TEM images of (1 0 1) and (1 1 1) oriented surfaces are also given in (c) and (d).

The symmetric deformation patterns on the indented surfaces have also been reported in some previous studies on fcc Cu single crystals [9,10] and a tetragonal γ-TiAl alloy [8]. From crystal plasticity finite element method (CP-FEM), Zambaldi et al. [8] predicted a pile-up inverse pole figure (IPF) in a tetragonal γ-TiAl alloy that fourfold in-plane symmetry in [0 0 1], twofold in [1 1 1], and twofold in [1 1 0]. Although diverse investigations such as 3-dimensional observation of the texture and microstructure below the indent were done in a single crystal (1 1 1) fcc Cu by Zaafarani et al. [9,10], pile-up IPF was not reported in fcc alloys.

TEM observations of cross-sectional specimens were additionally performed (see Fig. 4) because of unclear evidence of mechanical twinning on the SEM images of the indented surfaces. For a (0 0 1) grain, straight deformation patterns with many dislocations were observed in the bright-field TEM image (Fig. 4a). The selected area diffraction pattern (SADP) and dark field image of the deformation patterns of the (0 0 1) grain (Fig. 4b) clarified the existence of the mechanical twins. However, in (1 0 1) and (1 1 1) grains (see Fig. 4c and d), no evidence related to the mechanical twinning was found. This result is very similar to the compressive test result of high Mn austenitic steels in which mechanical twins were only observed in the [0 0 1]-oriented sample [1]. Therefore, the Schmid factor of compression can be one of the useful indicators for mechanical twinning occurring during nanoindentation tests.

However, it is still unclear when the mechanical twinning took place in (0 0 1) grains during the nanoindentation, because the TEM images of the mechanical twins were taken after the nanoindentation and the *P*–*h* curve of the (0 0 1) grain exhibits only one pop-in. Therefore, it is still difficult to judge whether the yielding of the (0 0 1) grain corresponding to the pop-in was caused by mechanical twinning or dislocation glide. Further studies are desirable on the yielding mechanism of the (0 0 1) grain, including the validity of the assumption that the critical resolved shear stresses for both slip and twinning are approximately the same.

4. Conclusions

In summary, the orientation-dependent yielding and indentation modulus in Fe–18Mn–0.6C–1.5Al TWIP steel were investigated through nanoindentation and EBSD experiments. The plane-strain modulus and maximum shear stress at the pop-in (probably corresponding to shear yield strength) increased with an order of (0 0 1), (1 0 1), and (1 1 1). The anisotropy of the plane-strain modulus depends on the anisotropy of Young's modulus. The anisotropy of maximum shear stress at the onset of the pop-in was explained by the change in Schmid factor. Deformation patterns on the indented surfaces having different orientations were found to be a good indicator for estimating the primary slip system. As expected from the Schmid factor, TEM observations confirmed that mechanical twins formed only under the indents of (0 0 1) grains, showing a similar orientation dependency to the uniaxial compression test results.

Acknowledgement

This study was supported by a grant from the Fundamental R&D Program for Core Technology of Materials funded by the Ministry of Commerce, Industry and Energy, Republic of Korea.

References

[1] I. Karaman, H. Sehitoglu, K. Gall, Y.I. Chumlyakov, H.J. Maier, Acta Mater. 48 (2000) 1345–1359.
[2] K.-T. Park, G. Kim, S.K. Kim, S.W. Lee, S.W. Hwang, C.S. Lee, Met. Mater. Int. 16 (2010) 1–6.
[3] P. Yang, Q. Xie, L. Meng, H. Ding, Z. Tang, Scripta Mater. 55 (2006) 629–631.
[4] L. Meng, P. Yang, Q. Xie, H. Ding, Z. Tang, Scripta Mater. 56 (2007) 931–934.
[5] J.J. Vlassak, W.D. Nix, J. Mech. Phys. Solids 42 (1994) 1223–1245.
[6] J.C. Stinville, C. Tromas, P. Villechaise, C. Templier, Scripta Mater. 64 (2011) 37–40.
[7] Y. Wang, D. Raabe, C. Klüber, F. Roters, Acta Mater. 52 (2004) 2229–2238.
[8] C. Zambaldi, D. Raabe, Acta Mater. 58 (2010) 3516–3530.
[9] N. Zaafarani, D. Raabe, R.N. Singh, F. Roters, S. Zaefferer, Acta Mater. 54 (2006) 1863–1876.
[10] N. Zaafarani, D. Raabe, F. Roters, S. Zaefferer, Acta Mater. 56 (2008) 31–42.
[11] S. Kang, Y.-S. Jung, J.-H. Jun, Y.-K. Lee, Mater. Sci. Eng. A 527 (2010) 745–751.
[12] K.L. Johnson, Contact Mechanics, Cambridge Univ. Press, Cambridge, 1985.
[13] B.-G. Yoo, K.-S. Kim, J.-H. Oh, U. Ramamurty, J.-I. Jang, Scripta Mater. 63 (2010) 1205–1208.
[14] J. Kim, B.C. DeCooman, Metall. Mater. Trans. A 42 (2011) 932–936.
[15] S. Shim, H. Bei, E.P. George, G.M. Pharr, Scripta Mater. 59 (2008) 1095–1098.
[16] H. Bei, Z.P. Lu, S. Shim, G. Chen, E.P. George, Metall. Mater. Trans. A 41 (2010) 1735–1742.
[17] I. Gutierrez-Urrutia, S. Zaefferer, D. Raabe, Mater. Sci. Eng. A 527 (2010) 3552–3560.